Photonic Bandgaps with Defects and the Enhancement of Faraday Rotation

M. J. Steel, M. Levy, and R. M. Osgood, Jr., *Fellow, IEEE*

***Abstract*—We investigate enhancement of magnetooptical rotation in periodic magnetic garnet thin-film stacks with defects using a combination of coupled-mode theory and matrix calculations. We prove that a combination of high rotation per unit length and high output is unattainable for a symmetric grating with a single central defect. We demonstrate that the addition of a second defect introduces sufficient degrees of freedom to allow high transmission for a much larger range of rotation angles than was previously possible. We present a number of designs with emphasis on achieving 45° rotation in very short propagation lengths.**

***Index Terms*—Faraday rotation, gratings, magnetooptical, photonic bandgaps (PBGs).**

I. Introduction

MAGNETOOPTIC materials are important in a number of branches of integrated optics. Prominent among these is the exploitation of magnetic garnets for the construction of integrated isolators [1]–[5]. These devices exploit the off-diagonal elements of the dielectric tensor in magnetic materials to produce either a nonreciprocal rotation of the plane of polarization (Faraday effect) or a nonreciprocal phase change. While many designs have been suggested and demonstrated, a cheap and practical integrated isolator is yet to appear, due to complications such as birefringence and polarization dependence. Alternatively, one might imagine heterogeneous integration of bulk-style isolators onto a chip. However, bulk isolators have lengths on the order of a millimeter, and without waveguiding, diffraction losses would be unacceptable. So a significant enhancement of the intrinsic Faraday rotation with a corresponding reduction in isolator lengths would be most desirable. Magnetooptical materials also exhibit the Kerr effect, that is, polarization rotation on reflection. Among other applications, this effect has been exploited in certain types of magnetooptical data storage disks, and for material characterization. In most cases, Kerr rotations are of the order of a fraction of a degree. Enhancement of Kerr rotation would thus allow better designs for existing applications and might open new possibilities, such as mirrors that rotate the reflected light, or in reflective nonreciprocal devices such as circulators.

Manuscript received January 6, 2000. This work was supported in part by DARPA/AFOSR under Contract F49620-99-1-0038, and in part by an NIST Advanced Technology Program under NIST Cooperative Agreement 70NANB8H4018.

The authors are with the Department of Applied Physics and Columbia Radiation Laboratory, School of Engineering and Applied Science, Columbia University, New York, NY 10027 (e-mail: mikes@cumsl.ctr.columbia.edu).

Publisher Item Identifier S 0733-8724(00)08074-9.

Another subject of fundamental importance in optics is the exploitation of periodic systems. One-dimensional (1-D) stacks or "gratings" have been employed as filters and mirrors for many years, and over the past decade optical fiber Bragg gratings have found innumerable applications as filters, sensors, and components of larger devices [6]. At the same time, great interest has been attracted by high-index contrast, two- (2-D) and three-dimensional (3-D) periodic structures, known as "photonic crystals" [7], [8] which can exhibit complete photonic bandgaps (PBGs). A special class of periodic structures are those with internal defects, in which the periodicity is broken at a localized point, perhaps by a "phase shift" or missing layer. Such structures have useful properties, notably the introduction of transmission resonances (associated with high-Q modes), into the otherwise reflective PBGs. Photonic crystals with defects are currently in vogue, but defects are also of great importance in 1-D geometries, notably in distributed feedback lasers, and very narrow-band fiber filters and sensors.

Recently, several groups have begun to study systems that combine magnetooptical rotation with the resonant effects of periodic structures. They have considered periodic thin-film stacks in which there are one or more defects, and for which at least one of the component materials is magnetic. It has been demonstrated theoretically [9]–[11] and experimentally [12] that for frequencies associated with a defect resonance, the rotation per unit length for both Faraday (transmission) and Kerr (reflection) effects can be significantly enhanced by propagation in such structures (see Fig. 1). Thus it may indeed be possible to construct shorter isolators or interesting reflective devices that rotate polarization.

From these initial studies, a number of important issues remain. The enhanced rotation is typically accompanied by a reduction in transmission for the Faraday effect or low reflection for the Kerr effect. Indeed, in the experiments of Inoue *et al.* [12], in which a single active magnetic layer is sandwiched in a periodic dielectric stack, the maximum Kerr rotation is associated with a minimum of reflection which limits its usefulness. Sakaguchi and Sugimoto [11] have observed that for the Faraday effect, the use of repeated identical substacks (see Fig. 2) with two or three defects allows the enhanced rotation to be accompanied by some improvement in transmission. However, they found improvements only for certain, apparently arbitrary combinations of substacks and the tradeoff between output and rotation, while somewhat reduced, was not eliminated. Other multiple-defect designs produced no improvement over the performance of a single defect. No physical explanation for these improvements or a systematic procedure for optimization was given. Finally, the theoretical

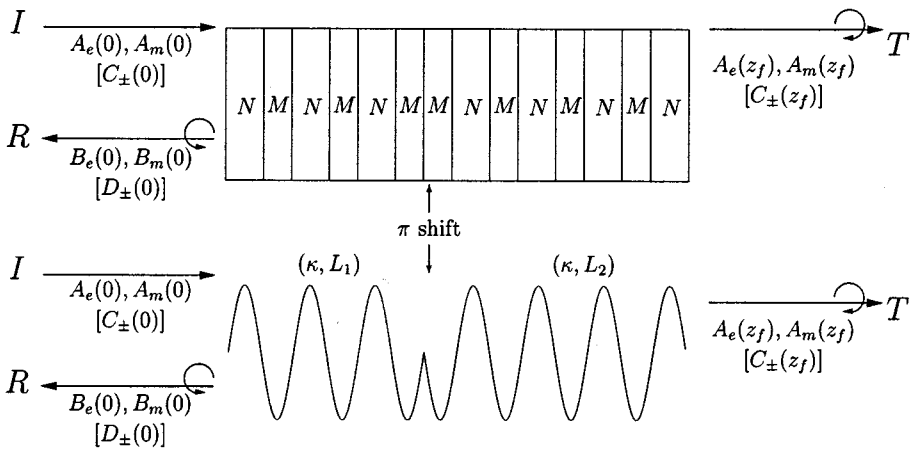

Fig. 1. Connection between thin-film stack and coupled-mode formalism. The upper panel shows a quarter-wave stack $(NM)^3(MN)^4$ of materials with refractive indexes M and N and the lower panel, a schematic representation of the corresponding coupled-mode picture. The incoming and outgoing fields are also indicated for both linear (A_e, A_m, B_e, B_m) and the corresponding circular polarizations $(C_\pm, D_\pm)$.

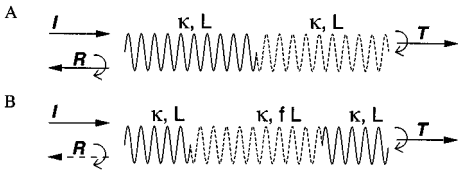

Fig. 2. General form of the two types of structures considered in the paper. A–Single symmetric defect. B–Two defects in length ratio $L : fL : L$. The dashed lines in each structure are used only to highlight the phase shifts. All structures have transmission T and reflection coefficients R, but for structure B we optimize for T only.

studies rely solely on the transfer matrix method. While this is an exact method for thin-film stacks, it provides little insight into the underlying reasons for the enhancement and is not easily extended to other geometries of importance for photonic integrated circuits, such as corrugated planar waveguides.

Recently, we studied a broader class of two-defect stacks in which the relative placement of the defects was allowed to vary [13]. We showed that using these designs, the tradeoff between rotation and transmission could be completely overcome, and explained how the optimum design could be found for a given desired rotation. The key to this procedure is to create an accidental degeneracy between transmission resonances for light of opposite circular polarization.

In the present work, we explore the properties of our proposed stacks in detail. We introduce a coupled-mode description that reduces the complex stack geometries to a few simple parameters, and thus highlights the essential physics much more clearly than a necessarily numerical implementation of the transfer-matrix method. It is thus easier to explain the enhancements and determine the best designs, and in some cases, we can extract simple analytic results. While the coupled-mode picture becomes inaccurate for systems with large index jumps, the insight and basic physical pictures established for the smaller index variation remain valid for high index contrast systems. In addition, a continuous picture such as a coupled-mode theory, allows us to vary certain parameters independently, whereas a matrix method entwines different aspects of the geometry together.

The paper is structured as follows. In Section II, we present the coupled-mode system for the periodic magnetic equations and discuss some properties of the uniform system and certain realizations. In Section III-A we explain the origin of the transmission–rotation tradeoff for one-defect systems. Proceeding to two-defect structures in Section III-B, we consider varying the position of the defects along the structure. We show for essentially any required rotation, there is a particular arrangement of the defects that gives high transmission from very short structures.

II. Model

The basic geometry is shown in Fig. 1. Linearly polarized light (I) is incident on a periodic structure that contains one or more defects. The structure may be a quarter-wave thin-film stack (upper half of Fig. 1), or a general periodic system (lower half). Due to the magnetic material in the system, the transmitted (T) and reflected (R) light is emitted with some rotation of the polarization θ and some ellipticity η. We wish to calculate these quantities for both the outgoing waves, aiming to find designs that produce a specified (large) rotation with as much energy as possible emitted in the desired mode (transmission or reflection) in a very short length. For most applications, notably isolators, we also require that the output field have negligible ellipticity.

A. Statement of the Problem and Dielectric Tensor

Our discussion is based on a coupled-mode treatment of a lossless magnetic medium with cubic crystal structure. A static magnetic field is applied in the propagation direction z to saturate the magnetooptic response and produces nonzero off-diagonal elements in the dielectric tensor $\epsilon_{xy} = -\epsilon_{yx} = i\epsilon_o$. These off-diagonal elements are, of course, the source of the magnetooptic rotation. A grating or periodicity is now introduced into

the problem. We allow both the diagonal and off-diagonal components to have periodic parts so that the dielectric tensor takes the form

$$\overleftrightarrow{\epsilon} = \begin{bmatrix} [\bar{\epsilon}_d + \epsilon'_d g(z)], & i[\bar{\epsilon}_o + \epsilon'_o g(z)], & 0 \\ -i[\bar{\epsilon}_o + \epsilon'_o g(z)], & [\bar{\epsilon}_d + \epsilon'_d g(z)], & 0 \\ 0, & 0, & \epsilon_{zz} \end{bmatrix} \quad (1)$$

where $g(z) = \cos[(2\pi z/\Lambda) + \delta]$. For a thin-film stack of alternating quarter-wave layers $HLHLHL\ldots$, this form for $\overleftrightarrow{\epsilon}$ is obtained straightforwardly by approximating the discrete periodic changes by their lowest order Fourier components. The period Λ is the length of a single unit HL while δ represents a possible phase shift. For moderate index differences, the restriction to two Fourier terms is an excellent approximation, provided we study frequencies close to the lowest Bragg resonance. The influence of higher Fourier components of the structure is largely felt at higher Bragg resonances. Note that we have assumed there is no birefringence between the x and y directions.

B. Coupled-Mode Equations

To derive a coupled-mode representation, the electric field at a wavelength $\lambda = 2\pi c/\omega$ is written as

$$\boldsymbol{E} = [(A_e(z)\hat{\boldsymbol{x}} + A_m(z)\hat{\boldsymbol{y}})\exp(i\pi z/\Lambda) + (B_e(z)\hat{\boldsymbol{x}} + B_m(z)\hat{\boldsymbol{y}})\exp(-i\pi z/\Lambda)]\exp(-i\omega t) + c.c. \quad (2)$$

In a uniform nonmagnetic medium, the amplitudes of forward-propagating (A_e and A_m) and backward-propagating (B_e and B_m) waves are constant. Here, the amplitudes are coupled by the periodic and magnetic parts of the dielectric tensor, and they acquire a z-dependence. Inserting (2) into Maxwell's equations and discarding nonphase-matched terms leads to the coupled system

$$\frac{d}{dz}\begin{bmatrix} C_+ \\ D_+ \\ C_- \\ D_- \end{bmatrix} = \begin{bmatrix} \mathsf{U}^+ & \mathsf{V} \\ \mathsf{V} & \mathsf{U}^- \end{bmatrix}\begin{bmatrix} C_+ \\ D_+ \\ C_- \\ D_- \end{bmatrix} \quad (3)$$

where $\mathsf{U}^{\pm}$ and V are 2×2 matrices, and we have expressed the problem in terms of the "circularly polarized" amplitudes

$$C_{\pm} = (A_e \mp iA_m)/\sqrt{2} \quad (4a)$$

$$D^{\pm} = (B_e \mp iB_m)/\sqrt{2}. \quad (4b)$$

The matrices $\mathsf{U}^{\pm}$ contain the familiar terms of the coupled-mode equations for contra-propagating systems

$$\mathsf{U}^{\pm} = i\begin{bmatrix} q_{\pm} & \kappa_{\pm}e^{i\delta} \\ -\kappa_{\pm}e^{-i\delta} & -q_{\pm} \end{bmatrix} \quad (5)$$

while for a nonbirefringent medium, the off-diagonal matrix $\mathsf{V} = 0$. Thus the circular modes of positive and negative sense of polarization are completely decoupled.

The parameters in (5) are defined in terms of a reference Bragg wavelength $\lambda_0 = 2\pi c/\omega_0$ and the mean index $\bar{n}(\omega_0)$ which together satisfy the standard Bragg relation

$$\lambda_0 = 2\bar{n}(\omega_0)\Lambda. \quad (6)$$

That is, in a uniform grating, light at the wavelength λ_0 is strongly Bragg-reflected. The mean index is trivially $\bar{n} = (n_1d_1 + n_2d_2)/\Lambda$ where the two types of layers have index $n_j = \sqrt{\epsilon_{xx,j}}$ and thickness $d_j = \lambda/(4n_j)$, while $\Lambda = d_1 + d_2$.

Returning to the other parameters in (5), $q_{\pm} = q \pm \alpha_0$, where $q = (\omega - \omega_0)\bar{n}/c$, represent wavenumber detunings from the Bragg resonance. The periodicity in the system couples the forward and backward modes with a strength given by $\kappa_{\pm} = \kappa \pm \alpha_1/2$, where κ is the contribution of the periodicity in the diagonal part of the dielectric tensor. For a stack with moderate index jumps, $\kappa \approx \pi(n_2 - n_1)/(2\bar{n}\lambda_0)$. Finally, the magnetic effects are expressed through the parameters $\alpha_0 = \pi\epsilon_o/(\bar{n}\lambda)$ and $\alpha_1 = \pi\epsilon'_o/(\bar{n}\lambda)$. The signs of α_0 and α_1 are determined by the sense of the applied static magnetic field.

1) Waveguides: With some minor adjustments in interpretation, the coupled-mode equations are, of course, also applicable to propagation in waveguides which have a periodicity introduced say, by surface corrugation. In this case, (1) is regarded as a description of the *effective* dielectric constant with the parameters determined by the details of the geometry, field polarization, and the shapes of the waveguide modes [14], the amplitude functions modulate transverse electric (TE) and transverse magnetic (TM) modes, rather than plane waves. Due to modal dispersion, the off-diagonal matrix V is no longer necessarily zero but takes the form

$$\mathsf{V} = i\begin{bmatrix} \Delta/2 & (\Delta\kappa/2)e^{i\delta} \\ -(\Delta\kappa/2)e^{i\delta} & -\Delta/2 \end{bmatrix} \quad (7)$$

where $\Delta = \beta_e(\omega_0) - \beta_m(\omega_0)$ is the difference in propagation constants of the TE and TM modes. The mean index becomes the mean *effective* index $\bar{n} = c(\beta_e + \beta_m)/(2\omega_0)$. The grating coupling is also different for each mode, so that $\kappa = (\kappa_e + \kappa_m)/2$ is now a mean coupling strength while $\Delta\kappa = \kappa_e - \kappa_m$ is the difference in the coupling coefficients. The values of all these parameters and the magnetic terms α_0 and α_1 depend on the shape of the waveguide modes. A nonzero matrix V complicates the solution of (3), and, in fact, strongly dispersive systems can destroy many of the properties we explore in the paper. For instance, if $\Delta \gg \alpha_0$, the resultant phase mismatch produces elliptical polarization of the transmitted light, and a dramatic decrease in the achievable Faraday rotation. Birefringence is indeed the major difficulty in constructing integrated isolators based on polarization rotation. It can be countered by techniques such as quasiphase matching [15] or compensation of modal birefringence with strain birefringence of opposite sign [16]. With careful waveguide and grating design we can also arrange for similar coupling coefficients $\kappa_{\mathrm{TE}} \approx \kappa_{\mathrm{TM}}$. Therefore, we assume throughout that the off-diagonal matrix $\mathsf{V} = 0$.

2) Solution to Coupled-Mode Equations: Equation (3) describes the field evolution in a uniform section of the grating of length L. With the assumption $\mathsf{V} = 0$, the solution relating the fields at the front ($z = 0$) and rear ($z_f = L$) is shown in (8) and (9) at the bottom of the next page where $\sigma_{\pm} = \sqrt{\kappa_{\pm}^2 - q_{\pm}^2}$. We choose a TE input of unit amplitude $A_e(0) = 1$ (see Fig. 1) so that $C_{\pm}(0) = 1/\sqrt{2}$, while the condition that no light enters from the rear of the grating gives $D_{\pm}(z_f) = 0$. Equation (8) is

then solved for the unknowns $C_\pm(z_f)$ and $D_\pm(0)$, to yield the transmission and reflection coefficients

$$t_\pm = \frac{C_\pm(z_f)}{C_\pm(0)} \tag{10a}$$

$$r_\pm = \frac{D_\pm(0)}{C_\pm(0)}. \tag{10b}$$

More generally, we are concerned with a series of gratings of length z_i, whose phase parameters δ (and perhaps other parameters), change in each section. Notably a "missing" layer in a stack corresponds to a shift in δ of π. The complete response is found from the product of the individual matrix operators $\mathsf{U}_i^\pm$ for each uniform grating

$$\begin{bmatrix} C_\pm \\ D_\pm \end{bmatrix}_{z=z_f} = e^{\mathsf{U}_n^\pm z_n} e^{\mathsf{U}_{n-1}^\pm z_{n-1}} \cdots e^{\mathsf{U}_2^\pm z_2} e^{\mathsf{U}_1^\pm z_1} \begin{bmatrix} C_\pm \\ D^\pm \end{bmatrix}_{z=0} \tag{11}$$

where $z_f = \sum_i z_i$ is the length of the entire structure. Equations (10) remain valid. In (11), it is assumed that the mean index is unchanged in adjacent gratings, which is the case for the problems we consider here. For structures with changes in the mean index, additional transition matrices are inserted between each propagation matrix $\exp(\mathsf{U}_i^\pm z_i)$ to account for Fresnel reflections [17].

At times, we also calculate the response of our structures using the transfer matrix method, which is exact for thin-film stacks. The procedure is analogous to the matrix concatenation for the coupled mode equations in (11), except that a separate matrix is required for each layer of the stack. The theory is well-known and the reader is referred elsewhere for details [10], [11], [18].

3) Basic Properties: We first summarize some properties of (3) for a single uniform grating. Due to the block-diagonal structure of (3), the response of the system may be considered separately for each sense of circular polarization. As the fundamental property of a periodic system, each pair of modes (+ or −), exhibits a PBG—incident light in the frequency range $|q_\pm| \le \kappa_\pm$ experiences strong reflection, while light outside the gap is largely transmitted. The reflectivity at $q_\pm = 0$ is given by $R = \tanh^2 \kappa_\pm L$, while the width of the band gap is $2\kappa_\pm$ and is approximately proportional to the strength of the index modulation. For nonmagnetic materials, the band center is given by the Bragg condition (6) corresponding to $q = 0$.

Expressing (3) in terms of circularly polarized modes has two advantages. First, the decoupling of the polarizations allows us to make simple interpretations of the system response to incoming linearly polarized light—we analyze each structure for its separate response to each circular polarization, and then combine the results using (4). Second, there is a clear separation of the effects of the two magnetic parameters α_0 and α_1. The detuning q which is associated with the *mean* refractive index is split by the mean magnetic strength α_0 into the quantities $q_\pm$, with $q_+ - q_- = 2\alpha_0$. In the absence of periodicity, the splitting of q_+ and q_- simply represents the magnetic circular birefringence which accounts for the normal Faraday rotation of linearly polarized light. Here, the splitting induces a separation between the centers of the band gaps for left- and right-circular polarization. Similarly, the grating strength κ which derives from the *periodic* part of the refractive index is split by the periodic magnetic coupling α_1. As a result, the two band gaps are not only shifted by the splitting $2\alpha_0$ but exhibit slightly different reflectivities. For realistic dielectric materials, $\kappa \gg (\alpha_0, \alpha_1)$ and the magnetic effects may be considered as perturbations to the influence of the grating. This is not necessarily true for metallic ferromagnets such as the cobalt layer used in [12].

C. Realistic Values and Dimensionless Units

We now describe our notation for different structures and give some realistic physical parameters. A grating structure is denoted by an expression of the form $(\kappa_1, L_1) : (\kappa_2, L_2) : \ldots$ indicating the coupling strength κ_j and length L_j of each section. A colon indicates a π phase shift. Discrete thin-film stacks are expressed as a sequence of repeated units such as $(MN)^l(NM)^m(MN)^n \ldots$, where M and N denote magnetic and nonmagnetic layers, respectively. All layers are quarter-wave plates of thickness $t = \lambda_0/(4n_j)$. The relation between the two pictures is indicated schematically in Fig. 1.

For physical values we choose a resonant frequency of $\lambda_0 = 1.55\ \mu$m and consider structures of either bismuth-substituted yttrium iron garnet (Bi-YIG) and gallium gadolinium garnet (GGG), or Bi-YIG and SiO_2. Bi-YIG is a favorable magnetic material as it has a high Faraday rotation, low loss at communications wavelengths, and may be integrated into circuits by sputtering or single crystal liftoff techniques [19], [20]. GGG is a convenient substrate for growing YIG. Alternatively, YIG may also be sputtered on to SiO_2 which makes for larger index contrasts and thus stronger resonant effects. The diagonal elements of the dielectric tensor have the values $\epsilon_{xx}^{\mathrm{YIG}} = 4.75$, $\epsilon_{xx}^{\mathrm{GGG}} = 3.71$, and $\epsilon_{xx}^{\mathrm{SiO_2}} = 2.25$. The off-diagonal element for Bi-YIG is $\epsilon_{xy} = 0.00269$ which corresponds to a Faraday rotation of $\theta_F = 0.48^\circ\ \mu\mathrm{m}^{-1}$. To obtain dimensionless units we normalize by $\gamma_0 = \pi\epsilon_{xy}/(\bar{n}\lambda_0)$, the intrinsic rotation per unit length of the magnetic material. For YIG/GGG stacks, $\gamma_0 = 0.00266\ \mu\mathrm{m}^{-1}$, and the normalized parameters are $\alpha_0 = 0.47$, $\alpha_1 = 0.626$, and $\kappa = 123$. This scaling is always used in the results below unless otherwise specified. For corrugated slab waveguides, the gratings have much weaker strength—the maximum attainable values are of order $\kappa_e, \kappa_m \lesssim 20$, while $\alpha_0 \approx 1$ and $\alpha_1 = 0$.

$$\begin{bmatrix} C_\pm \\ D_\pm \end{bmatrix}_{z=z_f} = e^{\mathsf{U}^\pm L} \begin{bmatrix} C_\pm \\ D_\pm \end{bmatrix}_{z=0} \tag{8}$$

$$= \begin{bmatrix} \cosh\sigma_\pm L + i\frac{q_\pm}{\sigma_\pm}\sinh\sigma_\pm L & i\frac{\kappa_\pm}{\sigma_\pm}\sinh\sigma_\pm L \\ -i\frac{\kappa_\pm}{\sigma_\pm}\sinh\sigma_\pm L & \cosh\sigma_\pm L - i\frac{q_\pm}{\sigma_\pm}\sinh\sigma_\pm L \end{bmatrix} \begin{bmatrix} C_\pm \\ D_\pm \end{bmatrix}_{z=0} \tag{9}$$

III. DEFECTS

As discussed earlier, several authors have predicted, and in one case measured, enhanced rotation both in transmission and reflection when a thin-film stack contains one or more defects. The basic explanation of the enhancement is simple. In a uniform magnetooptic medium (with the saturating magnetic field oriented longitudinally), the two circularly polarized modes are transmitted with a slightly different optical path length due to the magnetic circular birefringence. Incoming linear light, which excites equal contributions of the circular modes is therefore rotated. In a periodic system with one or more defects, transmission resonances appear inside the PBG. When illuminated with light near a resonant frequency, a large quantity of energy is stored inside the structure, strongly localized near the defects. The trapped light thus experiences an extended optical path length and there is an increase in the path *difference* between the two circularly polarized components over the path difference obtained on transmission through a uniform medium (or on reflection from a single interface). As a result, the overall Faraday or Kerr rotation is increased.

Such enhancements have been described for several types of hypothetical structures with different numbers of defects [9]–[12]. A single central defect has been found to improve rotation but at the cost of output intensity—a structure designed to achieve high rotation on reflection suffers from low reflectivity. Multiple defects have been found to help improve the output intensity in transmission. Up until our previous paper [13], however, no detailed physical picture of the enhancement (beyond the simple path difference description), or the role of multiple defects had been presented. In the following sections we discuss each of the structures shown in Fig. 2. We begin by providing a complete explanation of the single-defect tradeoff (Structure A). We then study two-defect systems for a broader class of structures than has been done previously and show how we can achieve new levels of optimization (Structure B).

In all cases, we consider rotation of incoming TE- or x-polarized light of unit intensity $|A_e(0)|^2 = 1$. Thus a pure TM (y) output represents $\pm 90^\circ$ rotation.

A. Single Symmetric Defect

Two types of thin-film stacks with a single defect have been studied previously. In one type, the structure consists of an equal number of alternating magnetic and nonmagnetic layers with a skipped middle layer in the form $(MN)^j(NM)^j$ or $(NM)^j(MN)^j$ [10], [11]. In the other type, the design is again symmetric but the middle magnetic layer may be extended and may be the only magnetic layer in the system [10], [12], for example, $(N_1N_2)^j(M)^k(N_2N_1)^j$. In transmission or Faraday mode, both these classes of structures show similar behavior: the rotation increases dramatically with the number of layers j, but the transmission simultaneously decreases. In the reflection or Kerr mode, there is a similar tradeoff between the rotation and the reflectivity. In the experiment of [12], for example, Kerr rotations of up to 10° were recorded, but each enhancement was associated with a minimum of the reflectivity, which was less than 1% for the highest rotation. Here we investigate whether this tradeoff can be overcome.

The coupled-mode version of the skipped layer stacks is the simple structure $(\kappa, L) : (\kappa, L)$—two identical gratings with a central π phase shift (see Fig. 2, Structure A). The properties of such a structure without magnetic effects are well known—the gratings produce a band gap while the defect induces a perfect transmission resonance at the center of the band gap with a bandwidth that decreases exponentially with κL [21]. Phase shifts other than $\delta = \pi$ produce similar resonances located away from the band center. Throughout this paper, we consider only symmetric π shifts for the sake of symmetry and to limit the parameter space.

The coupled-mode equations for this problem with the magnetic effects included are easily solved using (11); the manipulations can be simplified by the use of an effective medium picture [17]. The individual transmission coefficients for each circular polarization [see (10)], are

$$t_\pm = |t_\pm| e^{i\phi_\pm} = \frac{-i(\kappa_\pm^2 - q_\pm^2)}{q_\pm^2 \cosh(2\sigma_\pm L) + iq_\pm\sigma_\pm \sinh(2\sigma_\pm L) - \kappa_\pm^2} \tag{12}$$

where $\sigma_\pm = \sqrt{\kappa_\pm^2 - q_\pm^2}$. For a strong grating in the vicinity of the resonance at $q_\pm = 0$, we have $\kappa_\pm \gg q_\pm$ and $\sigma_\pm \to \kappa_\pm$ so that the amplitude transmission coefficients reduce to the simple forms

$$t_\pm \approx \frac{i}{1 - (iq_\pm/2\kappa_\pm)\exp(2\kappa_\pm L)]}. \tag{13}$$

Similarly, we can find limiting forms for the reflection coefficients

$$r_\pm = |r_\pm| e^{i\psi_\pm} \approx \frac{i}{1 + (2i\kappa_\pm/q_\pm)\exp(-2\kappa_\pm L)}. \tag{14}$$

From these relations and (4) and (10), we find the parameters of main interest: the total transmission and reflection

$$T = |A_e(z_f)|^2 + |A_m(z_f)|^2 \qquad R = |B_e(0)|^2 + |B_m(0)|^2 \tag{15}$$

the Faraday (F) and Kerr (K) rotations

$$\theta_{F,K} = \frac{1}{2}\tan^{-1}\frac{2\,\mathrm{Re}\,(\chi_{F,K})}{1 - |\chi_{F,K}|^2} \tag{16}$$

and the corresponding ellipticities

$$\eta_{F,K} = \tan\left[\frac{1}{2}\sin^{-1}\left(\frac{-2\,\mathrm{Im}\,(\chi_{F,K})}{1 + |\chi_{F,K}|^2}\right)\right]. \tag{17}$$

Here $\chi_F = A_m(z_f)/A_e(z_f)$ and $\chi_K = B_m(0)/B_e(0)$. Note that when $|t_+| = |t_-|$, the transmitted light is linearly polarized $(\eta_F = 0)$ with $\theta_F = -(\phi_+ - \phi_-)/2$. Similarly, $\theta_K = -(\psi_+ - \psi_-)/2$ when $|r_+| = |r_-|$.

Fig. 3 presents typical results for a single symmetric defect using YIG/GGG parameters (see Section II-C). The spectral responses for circular and linear polarizations are given in the upper and lower panels, respectively. We remind the reader that the two circular modes act independently and that the linear response is to be considered as the summed effect of the two circular polarization responses. The upper panel shows the trans-

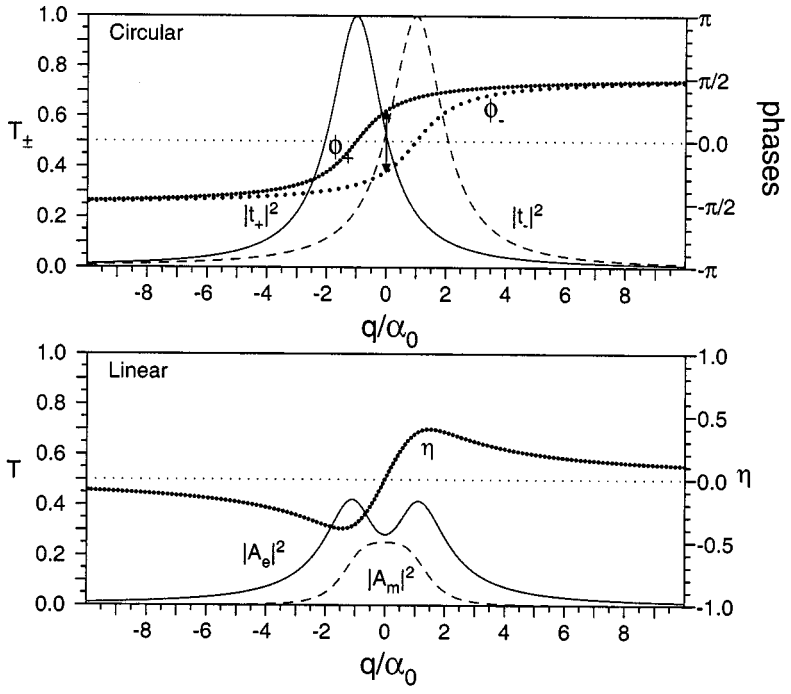

Fig. 3. Response of a symmetric grating with a central π phase shift. $\kappa = 123$, $\alpha_0 = 0.47$, $\alpha_1 = 0.626$, and $L = 0.0252$. Upper panel: Transmission and phase of circularly polarized modes: $|t_+|^2$ (solid), $|t_-|^2$ (dashed), ϕ_+ (fine dotted), and ϕ_- (coarse dotted). Lower panel: Transmission of linearly polarized modes $|A_e(z_f)|^2$ (solid), $|A_m(z_f)|^2$ (dashed), and ellipticity η (dotted).

mitted intensities $T_\pm = |t_\pm|^2$ (solid and dashed lines) and phases $\phi_\pm = \arg(t_\pm)$ (dotted lines) according to (12) as a function of the detuning q/α_0. Each circular component sees an identical transmission resonance with the general Lorentzian form indicated by (13). Due to the circular magnetic birefringence, the resonances are separated in frequency by $2\alpha_0$. (Note that with $\kappa = 123$, the edges of the reflection band are far outside the domain of the figure and we see only the central resonances.) In the vicinity of each resonance, the associated phase (dotted lines) increases by π. At $q = 0$, the transmitted intensities are the same and the phase difference $\Delta\phi = \phi_+ - \phi_-$ has a maximum (indicated by the vertical arrow). The lower panel shows the transmission for the linearly polarized modes which is obtained from the results in the upper panel using (4a). The greatest rotation, i.e., the greatest conversion into the TM polarization (dashed line), occurs at the band center $q = 0$, where both circular components are transmitted with equal intensity and the phase difference $\Delta\phi$ is largest. Note, however, that the total transmitted intensity $T = |A_e(0)|^2 + |A_m(0)|^2 < 0.6$. The dotted line in the lower panel denotes the ellipticity η_F. The ellipticity η_F (dotted line) vanishes at $q = 0$ where the circular modes are transmitted equally, but is nonzero elsewhere.

Fig. 4 shows the response of the same system with the length increased to $L = 0.03$. In accord with (13), the bandwidth of the resonances is smaller (corresponding to the increase in the Q-factor of the resonance). Further, the phase functions $\phi_\pm$ are more step-like, with their variation localized about the points $q_\pm = 0$, respectively. This causes an increase in the phase difference $\Delta\phi(q = 0)$, and thus in the rotation. However, the narrowing of the resonances also leads to a decrease in the total transmission at band center, because the point $q = 0$ now lies further into the wings of each resonance. There is thus a basic compromise between the rotation and the transmission. Similar arguments based on (14) show that such a tradeoff also occurs with the rotation of reflected light.

Indeed, in the limit $\kappa \gg \alpha_0, \alpha_1$ (which is invariably true for garnets), (13)–(15) lead, after a little algebra, to the relations

$$T = 1 - R = (1 + \rho^2)^{-1} \tag{18}$$

$$\theta_F = \frac{\pi}{2} - \theta_R = \tan^{-1}(\rho) \tag{19}$$

where

$$\rho = \frac{\alpha_0 \exp(2\kappa L)}{2\kappa} \tag{20}$$

or simply

$$T = \cos^2\theta_F \qquad R = \cos^2\theta_R. \tag{21}$$

Equation (21) states that an increase in rotation directly implies a reduction in output intensity for both transmissive and reflective modes of operation. This system simply has insufficient degrees of freedom to be optimized for both large rotation and significant optimization. For thin-film stacks with large index variation, the precise results depart from these relations, but the basic tradeoff remains and may be confirmed by matrix calculations. Thus the low output observed in the experiments of [12] is now seen as a result of the competing demands placed on the shapes of the resonances for the circularly polarized modes—we cannot simultaneously obtain a broad resonance needed for high output and large phase difference needed for high rotation. We conclude that a structure based on a single symmetric defect is not suitable for efficient, high-output devices.

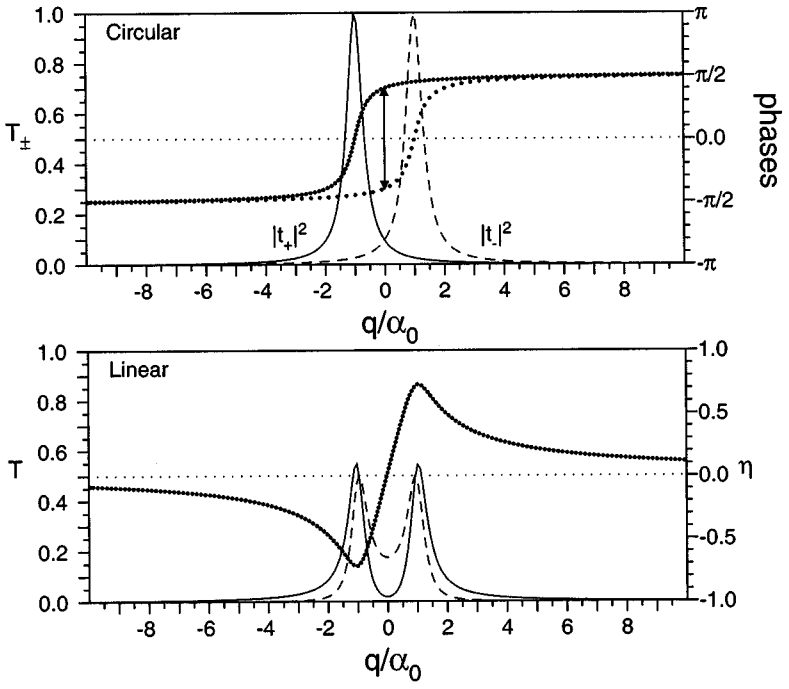

Fig. 4. As for Fig. 3 with $L = 0.03$.

B. Two Defects in Transmission

With the limited possibilities of a single defect, the introduction of an additional phase shift is now motivated by the need to introduce extra degrees of freedom. Sakaguchi and Sugimoto [11] have considered designs in which two defects are placed at one quarter and three quarters of the way through the stack, for example, $(MN)^j(NM)^{2j}(MN)^j$. Thus the lengths of each section are in the ratio $L : 2L : L$. They showed that with such designs the rotation can be maintained with some degree of improvement in transmission, up to a maximum of 95%, but for each design, high transmission occurred only for a particular value of j. They found some further improvements with three-defect structures of the form $L : 2L : 2L : L$. However, a fundamental problem remains. The transmission and rotation cannot be controlled independently—the number of repetitions j is determined by the requirement of achieving high transmission, and one is left with whatever rotation the system generates. In particular, the maximum transmission for rotations close to 45°, which are important for isolator applications, was ≈75%-80%.

Recently, we suggested using a broader class of two-defect structures of the form $(MN)^j(NM)^k(MN)^j$ where $j \leq k \leq 2j$ [13]. Our preliminary results showed significant advances. By varying the ratio k/j we were able to obtain high transmission for essentially any desired rotation, overcoming the tradeoff we have discussed earlier. Here we explore these designs in greater detail using the perspective of the coupled-mode theory. In the coupled-mode description, the analogous structures have their lengths in the ratio $L : fL : L$ where $f \in [1, 2]$ is a free parameter corresponding to the ratio k/j (see Fig. 2, Structure B). Note that with this form for the gratings, we introduce more flexibility into the designs than considered by others, yet retain a high degree of symmetry. The coupled-mode results then allow us to explain why the earlier multiple defect designs [11] (for which $f = 2$), exhibited an improvement over the single-defect design. Moreover, we demonstrate that the freedom introduced by the parameter f allows the improvement in transmission to be tuned over a much wider range of rotation angles again. Finally, the coupled-mode description allows us to separate the roles of the scale length L and the length ratio f. By contrast, when modeling discrete stacks [13], the addition of a single layer changes both the overall length and the relative sizes of each section, which complicates the interpretation of results.

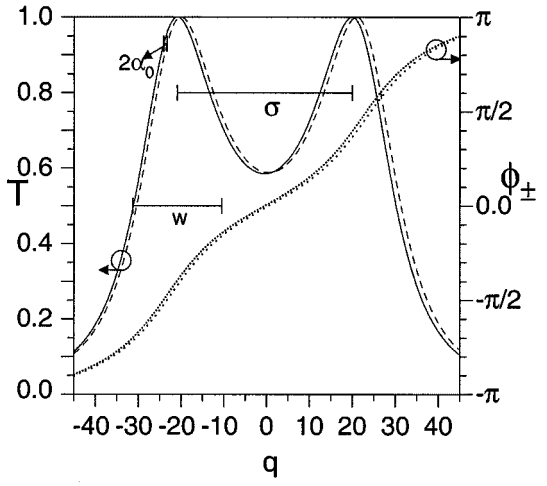

Fig. 5. Circular polarization transmission spectra of a two-defect system with $L = 0.0103$, $f = 1.4$, and $\kappa = 123$. Line styles denote transmission T for C_+ (solid) and C_- (dashed), and phases ϕ_+ (fine dotted) and ϕ_- (coarse dotted).

1) Resonance Structure: Optimization of our two-defect system is again simplified by considering the combined effects of the independent transmission resonances for each circularly

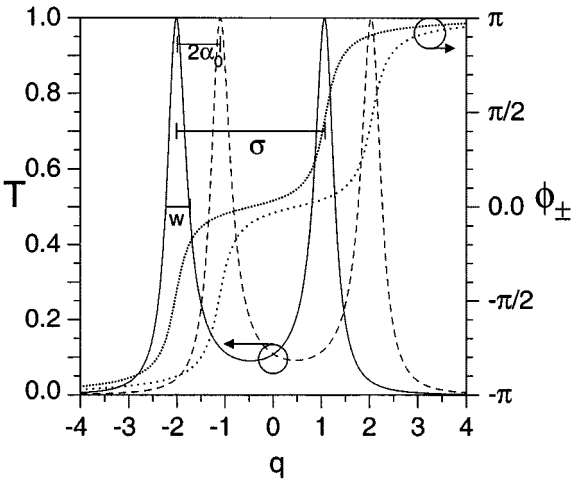

Fig. 6. As for Fig. 5 with $L = 0.0253$. Note the decreased scale for the x-axis.

polarized mode. To indicate the typical form of the resonances, in Fig. 5 we show the response according to the coupled-mode equations for a system with $f = 1.4$ and $L = 0.0103$. Fig. 6 also shows the response for $f = 1.4$, but with a larger length $L = 0.0253$. For both figures, the various line styles have the same interpretation as for the upper panel of Fig. 3, i.e., circular transmissions as solid and dashed lines, and the corresponding phases as dotted lines. The obvious manifestation of the extra defect is an additional transmission resonance for each mode.

Using Figs. 5 and 6, we attempt optimization by analyzing how the resonance structure changes with the length L and ratio f. The relevant coupled-mode system can be solved analytically, but in practice the exact solutions are rather unwieldy, and are no more useful than numerical solutions to the coupled-mode equations. However, from basic physics arguments and study of the numerical results, we can make the following general conclusions about the behavior of the system as f and L vary. Note the labeled arrows in Figs. 5 and 6, indicating the splitting of each peak σ, a rough estimate of the peak width w, and the magnetic splitting $2\alpha_0$.

1) As there are two defects in the structure, we observe two transmission resonances (the case $f = 2$ is an exception we discuss later). There is a phase increase of π in the vicinity of each resonance, so that in traversing both resonances the phase is advanced by 2π. The two resonances are simply symmetric and antisymmetric splittings of the single resonance introduced by each defect.
2) For $f \leq 2$, we find that the maximum transmission of each peak is always unity and the response is symmetric around $q_{\pm} = 0$.
3) Just as for the single-defect problem, the separation $2\alpha_0$ between the two polarization modes is a constant, fixed by the magnetooptical strength of the materials. The peak width w and separation σ for a single mode, however, depend on the parameters f and L.
4) For very short lengths L, the structures have a low-quality factor Q and the peak width $w \gg 2\alpha_0$ is so broad that the peaks for each polarization overlap and the phase difference $\phi_+(q) - \phi_-(q)$ is very small. This is the situation in Fig. 5, for $f = 1.4$ and $L = 0.0103$.
5) As L is increased, we find two general effects:
   - the width w of each peak decreases.
     This is the familiar line-narrowing due to the increasing Q-factor of the structure, just as with the single-defect gratings in the previous section. The situation of Fig. 5 is transformed to more closely resemble that of Fig. 6.
   - the separation σ of the two peaks also decreases.
     This corresponds to a reduction of the splitting in the symmetric and antisymmetric modes, as the two defects are pulled further apart, and interact less strongly. In the limit of infinite L, the interaction vanishes and the two peaks become degenerate.
6) The width w obtained for a given separation σ increases with f.
   This may be observed in Fig. 7(a) and (b) which are exact analogues of Fig. 3. We concentrate on just the solid line in the upper panels representing the transmission of one circular polarization. For $f \lesssim 1.5$ (see Fig. 7(a) with $f = 1.5$), the two peaks are still relatively well resolved. As f increases, the width for the same separation σ increases, and the peaks become less distinct (see Fig. 7(b) for which $f = 1.88$). Finally, at $f = 2$, the two peaks coalesce into a single broad resonance.

2) Optimization with Two Defects: We are now in a position to understand the new possibilities for optimization with two defects. We consider Fig. 6 again, and analyze the combined action of the transmission spectra for both polarizations (i.e., both solid and dashed lines). As observed in the previous section, if the length scale L is increased for a fixed value of f, the splitting σ decreases while the magnetic separation $2\alpha_0$ remains fixed. Hence for a certain value of L, the rightmost resonance of C_+ (solid line in Fig. 6) and the leftmost resonance of C_- (dashed line) can be "dragged through" each other. Thus we create an accidental degeneracy where the peaks coincide at $q = 0$. At such a point, we expect perfect transmission but also a large phase difference because the phases of the coincident resonances have opposite parity. This situation is shown in the upper panels of Fig. 7, where the length in each case was chosen carefully to obtain the accidental degeneracy. The plots show the circular polarization response for $f = 1.5$ [Fig. 7(a)], and $f = 1.88$ [Fig. 7(b)]. In each plot, there is a large phase difference $\phi_+ - \phi_-$ at $q = 0$, while the transmission coefficients are both unity. In the lower panels, which show the corresponding linear polarization response, we see that a significant fraction of the transmitted light at $q = 0$ is TM-polarized, and that the sum of the TE and TM transmitted light is virtually 100%. Also, as the two circular components are equally transmitted, the ellipticity η (dotted line) vanishes for $q = 0$.

These plots also illustrate the importance of varying the ratio f, in that the shape of the phase profiles ϕ_+ and ϕ_- are quite different for the two cases. For $f = 1.5$ [Fig. 7(a)], the two resonances of each single component are well differentiated and most of the variation in ϕ_+ and ϕ_- is localized around the peaks. The phase difference $\Delta\phi = [\phi_+(0) - \phi_-(0)] \approx \pi$ and we ob-

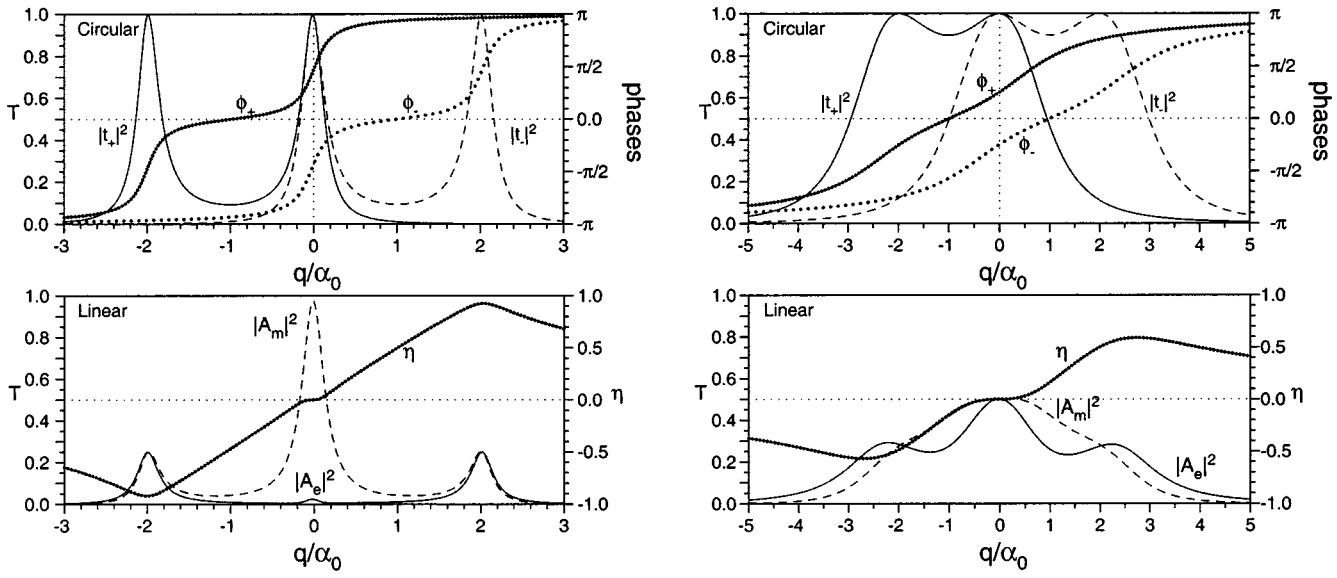

Fig. 7. Response of two-defect system for (a) $f = 1.5, L = 0.0301$ and (b) $f = 1.88, L = 0.0226$. Other parameters are $\kappa = 123$, $\alpha_0 = 0.47$, and $\alpha_1 = 0.626$. Upper panels show response for circular polarization components, lower panels for linear polarization. Line styles are the same as in Fig. 3.

tain a rotation close to -90° in the lower panel. By contrast, for $f = 1.88$ [Fig. 7(b)], the transmission peaks for a single circular component are strongly overlapping. The phase variation is more evenly distributed across the width of the whole resonance and so the phase difference $\Delta\phi(0)$ is smaller. The lower plot indicates the Faraday rotation obtained at $q = 0$ is -45° (equal output of TE and TM light).

Thus by selecting f and L correctly we can produce an accidental degeneracy between the two circular polarizations that generates both rotation of the desired angle, and close to perfect transmission. For the Bi-YIG/GGG parameters, the structures in the two figures have total physical lengths of 39.6 μm and 33.0 μm, respectively. For comparison, the same rotations would be obtained in a uniform slab of Bi-YIG with lengths of 591 μm and 295 μm, a factor of 10 or more larger. The ability to create nonreciprocal, high transmission rotations of 45° in a short distance is of great importance for constructing isolators and hence the example of Fig. 7(b) is of particular note.

3) Length Dependence: To illustrate the length dependence of these structures, Figs. 8(a) and (b) show the properties at band center $q = 0$ as a function of the total device length $L_{\rm tot} = (3+f)L$. We take the same two values of f as in Fig. 7, plotting the total transmission $T = |A_e(z_f)|^2 + |A_m(z_f)|^2$ (solid lines), rotation θ_F (dashed), and ellipticity η (dot-dashed) obtained from solution of the coupled-mode equations. The vertical dotted lines indicate the lengths at which the accidental degeneracy is obtained, and thus correspond to the $q = 0$ values in Figs. 7. (The discrete points marked $+$ and $\times$ are obtained from thin-film matrix calculations and are discussed later.) We discuss the transmission (solid line) first, concentrating on Fig. 8(a). For $L_{\rm tot} < 5$ μm, the total transmission is high, as the transmission resonances for C_+ and C_- are broad and overlapping (see item 4) in Section III-B1 and Fig. 5). However, the phase profiles are very similar, so the rotation is small. As $L_{\rm tot}$ increases, the resonances sharpen (see item 5) in Section III-B1) to resemble the situation in Fig. 6 and the transmission at $q = 0$ therefore falls. The transmission briefly rises to unity at $L = 39.6$ μm as the peaks of opposite polarization pass through each other [the situation in Figs. 7(a)], and finally drops permanently once the splitting $\sigma < \alpha_0$ and the peaks are unable to interact at all. A similar form is seen for the transmission with $f = 1.88$ [Fig. 8(b)] but with a much less pronounced dip in the transmission around $L = 25$ μm. This is in accord with the relative shapes of the resonances in Figs. 7. The sharper resonance peaks seen for $f = 1.5$ [Fig. 7(a)] as compared to $f = 1.88$ [Fig. 7(b)] lead to the more dramatic changes in the transmission as a function of length. In general, the tuning tolerances in length are tighter for smaller values of f.

Turning to the rotation (dashed line) in Fig. 8, in both cases it increases monotonically with length as the resonance peaks become more defined and the phase profiles more step-like (compare the phase profiles in Figs. 5 and 6). It is also apparent that the rotation which occurs at optimum transmission may be controlled by choosing f—we obtain $\theta_F \approx 87^\circ$ for $f = 1.5$ and $\theta_F \approx 45^\circ$ for $f = 1.88$. In general, larger rotations are optimized for smaller values of f.

The dot-dash lines visible near the bottom of each part of Fig. 8 show the ellipticity at $q = 0$. If we had taken $\alpha_1 = 0$, both circular components would be equally transmitted at $q = 0$ and, consequently, the ellipticity would be identically zero. To best represent the Bi-YIG/GGG system, our results are shown for $\alpha_1 = 0.626$, which as discussed in Section II-B3 leads to slightly different reflection coefficients for the two circular components and creates a nonzero ellipticity. In both cases in Fig. 8, the ellipticity is very small until the system passes the point of maximum transmission.

4) Discrete Systems: To this point, we have assumed that we can choose lengths L and ratios f completely freely.

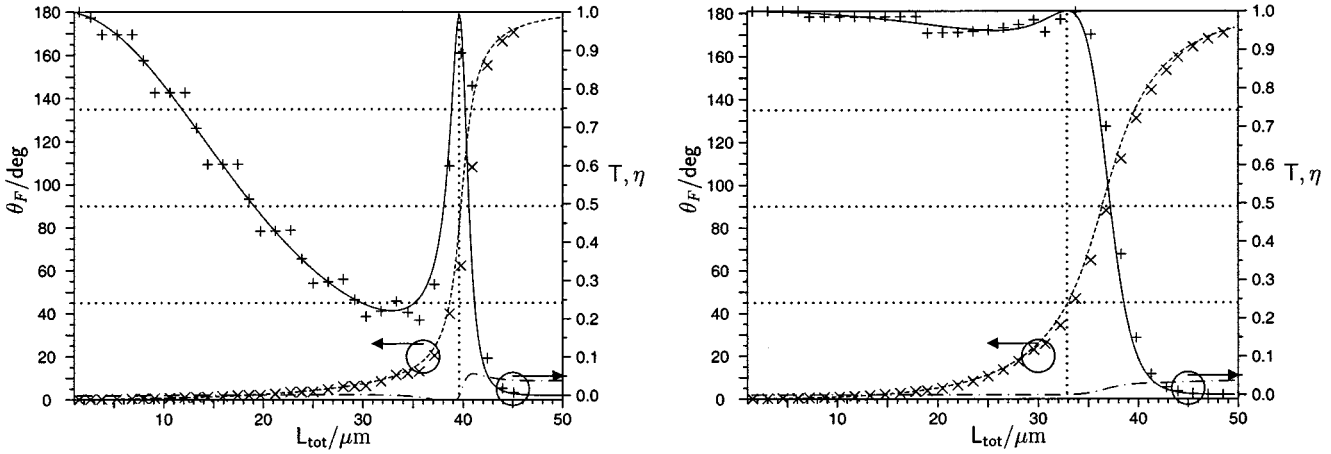

Fig. 8. Output as a function of system length for (a) $f = 1.5$ and (b) $f = 1.88$; other parameters as in Fig. 7.

For high index-contrast thin-film stacks, however, the length change upon adding a single layer is significant and in general we can only obtain discrete values of L and f. These values may not coincide precisely with the optimal values suggested by the continuous coupled-mode picture. This problem is illustrated by the $+$ and $\times$ symbols in Fig. 8, which show the results of matrix method calculations for YIG/GGG stacks. The stack structures were of the form $(NM)^j(MN)^k(NM)^j$, where the repetition numbers j and k were selected to match the desired values of f and L as closely as possible. The stack results cluster around the continuous results, but due to the discreteness, there are significant gaps between adjacent points. This issue is a particular problem near the transmission resonances. Examining the narrow peak of the transmission curve in Fig. 8(a), we see that the addition of a single layer causes the discrete transmission to jump from one side of the peak to the other, with a maximum of only $T = 0.89$. As in the previous section, these tolerance problems are tighter for lower values of f. If materials with larger index jumps were used in order to reduce the stack length, this problem would become even more acute.

Fig. 9 shows how this problem may be countered. The plot shows the peak transmission (solid) and rotation (dashed) as a function of f for the coupled-wave picture corresponding to YIG/GGG parameters. At every value of f, the length L has been chosen to optimize the transmission. [The slight drop in transmission to around 0.99 for small values of f is another consequence of the nonzero α_1 (see final paragraph of Section III-B2). Nonetheless, the coupled-mode theory curves predict that a wide range of rotations can be obtained with very high transmission. Consider now the discrete points which indicate thin-film stack realizations close to the continuous parameters. The open symbols denote the transmission which largely exceeds 0.99. The closed symbols indicate the rotation at $q = 0$. To increase the number of discrete rotations available, we have allowed the refractive index of the GGG layers to take on three different values. The circles denote stacks with the normal value $n = 1.926$, whereas the squares and diamonds denote realizations in which the GGG index has been reduced by 0.0025 and 0.005, respectively. Changes of this order could be created by stoichiometric adjustments. By allowing these small index variations, we can "fill in" some of the gaps observed in Fig. 8; if the addition of a single layer causes one realization to jump from one side of the transmission peak to the other, a stack with a slightly different GGG index may exhibit close-to-perfect transmission with a similar rotation. The dense clustering of points in Fig. 9 shows that by varying f we can indeed obtain virtually any desired rotation with high transmission over very short distances.

We have also performed calculations for the higher index-contrast YIG/SiO_2 system with the aim of optimizing transmission for a rotation of 45°—the most interesting rotation for the purpose of constructing isolators. The small number of layers in these systems makes it difficult to achieve transmissions as favorable as with YIG/GGG. For a structure $(NM)^9(MN)^{17}(NM)^9$ we obtain a rotation of $\theta_F = 44.9°$ with transmission $T = 98.4\%$, where M denotes a YIG layer, and N a SiO_2 layer with refractive index 1.495. The total length of the structure is $L_{\rm tot} = 15.3\ \mu$m. These values assume an external medium with a refractive index of 1.78, equal to the mean index of the stack so as to reduce Fresnel reflections. If the external medium is taken as air we obtain $\theta_F = 44.9°$ and $T = 92.4\%$, assuming the refractive index of the silica layer is adjusted slightly to 1.498. These values represent a considerable improvement over the $\approx 75\%$ transmissions obtained in [11].

Finally, in Fig. 9, we have also indicated the bandwidth $\Delta\nu$ of the resonances (dotted line) where the bandwidth is arbitrarily defined to be the range over which the rotation varies by less than 1°. We have also checked that over this bandwidth, the ellipticity is always well below $\eta = 0.01$. As expected for highly resonant structures, the bandwidth is relatively narrow, especially for high rotations, but should be sufficient for single-channel operation. It would clearly be impossible to use a single device for many wavelength-division multiplexing (WDM) channels.

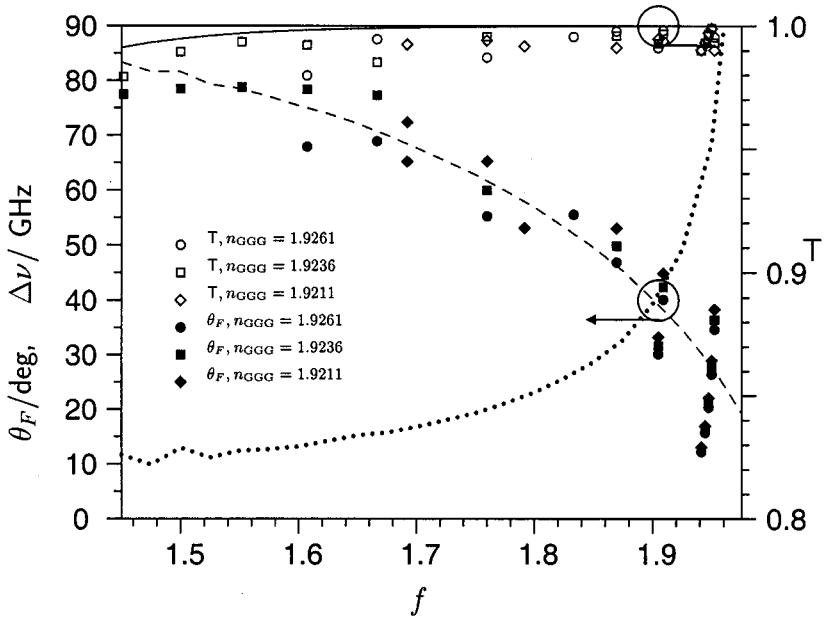

Fig. 9. Optimum transmission (solid) and rotation (dashed) according to the coupled-wave model for YIG/GGG parameters. Open and closed symbols correspond to transmission and rotation for individual stack realizations. Transmission bandwidth is shown as the dotted line.

C. Discussion and Conclusion

In demonstrating the existence of an optimum length L for each f, we have explained the improvement in performance predicted for two-defect systems in [11] as a particular case when $f = 2$ (see start of Section III-B). In that work it was found that high transmission only occurred if a certain number of layers j was used. This number of layers j is now clearly seen to be equivalent to the length L that optimizes the overlap of the transmission peaks for each circular polarization with a large phase difference. In fact, the case $f = 2$ is not an ideal choice for optimization. For $f = 2$, numerical solutions show that the two peaks in the transmission spectrum coalesce into a single broad peak with perfect transmission only at the center points $q_{\pm} = 0$. This is natural when it is realized that a structure with $f = 2$ can be considered as a concatenation of two identical gratings each with central phase shifts. Each individual grating is perfectly transmitting at $q = 0$, and so there must also be a peak at $q = 0$ for the whole structure. Due to the magnetic splitting, these peaks can never perfectly coincide and so 100% transmission is impossible for designs with $f = 2$. Nevertheless, the overlapping peaks are much broader than for the single-defect case, allowing a large phase difference while still achieving quite high transmission.

Finally, it was shown in [11] that concatenations of three identical structures performed even better than the doubly concatenated structures. Observing the impressive performance of the broader class of two-defect structures in this paper, it is interesting to ask whether there is still an advantage in adding further defects. The parameter space becomes too large for an exhaustive characterization but we have examined the performance of three-defect structures of the form $L : fL : fL : L$. We find that if we restrict only to structures with $f = 2$, there is indeed an improvement in transmission with three defects over two as previously observed [11]. However, if f is allowed to vary as in the present paper, our calculations show that a shorter two-defect structure can always be found that produces the same rotation with a larger bandwidth of operation and a transmission at least as great.

In summary, we have found that the addition of a second defect dramatically improves upon the results of a single defect. With the extra defect, we can arrange for an accidental degeneracy between transmission peaks for the different circular polarizations. The degeneracy provides high transmission while the opposite parity of the overlapping peaks produces the high rotation. By separately tuning the length L and spacing of the defects (through the ratio f), we break the tradeoff between transmission and rotation, so that the system may be optimized for a large range of angles. Such designs should increase the practicality of free-propagation integrated isolators by significantly reducing diffraction losses. In a subsequent paper, we will consider similar questions for enhanced Kerr rotation.

REFERENCES

[1] R. Wolfe, J. J. F. Dillon, R. A. Lieberman, and V. J. Fratello, "Broadband magneto-optic waveguide isolator," *Appl. Phys. Lett.*, vol. 57, p. 960, 1990.

[2] M. Levy, I. Ilic, R. Scarmozzino, R. M. Osgood, Jr., R. Wolfe, C. J. Gutierrez, and G. A. Prinz, "Thin-film-magnet magnetoopic waeguide isolator," *IEEE Photon. Technol. Lett.*, vol. 5, pp. 198–200, 1993.

[3] M. Levy, R. M. Osgood, Jr., H. Hegde, F. J. Cadieu, R. Wolfe, and V. J. Fratello, "Integrated optical isolators with sputter-deposited thin-film magnets," *IEEE Photon. Technol. Lett.*, vol. 8, pp. 903–905, 1996.

[4] J. Fujita, M. Levy, R. Ahmad, M. Randles, R. M. Osgood, Jr., C. Gutierrez, and R. Villareal, "Observation of optical isolation based on nonreciprocal phase shift in a Mach Zehnder interferometer," *Appl. Phys. Lett.*, vol. 75, pp. 998–1000, 1999.

[5] N. Bahlmann, V. Chandrasekhara, A. Erdmann, R. Gerhardt, P. Hertel, R. Lehmann, D. Salz, F.-J. Schröteler, M. Wallenhorst, and H. Dötsch, "Improved design of magnetooptic rib waveguides for optical isolators," *J. Lightwave Technol.*, vol. 16, pp. 816–823, 1998.

[6] R. Kashyap, *Fiber Bragg Gratings*. San Diego, CA: Academic, 1999.

[7] E. Yablonovitch, "Inhibited spontaneous emission in solid-state physics and electronics," *Phys. Rev. Lett.*, vol. 58, pp. 2059–2062, 1987.
[8] J. D. Joannopoulos, R. D. Meade, and J. N. Winn, *Photonic Crystals: Molding the Flow of Light*. Princeton, NJ: Princeton Univ. Press, 1995.
[9] M. Inoue and T. Fujii, "A theoretical analysis of magnetooptical Farday effect of YIG films with random multilayer structures," *J. Appl. Phys.*, vol. 81, pp. 5659–5661, 1997.
[10] M. Inoue, K. Arai, T. Fujii, and M. Abe, "Magnetooptical properties of one-dimensional photonic crystals composed of magnetic and dielectric layers," *J. Appl. Phys.*, vol. 83, pp. 6768–6770, 1998.
[11] S. Sakaguchi and N. Sugimoto, "Transmission properties of multilayer films composed of magnetooptical and dielectric materials," *J. Lightwave Technol.*, vol. 17, pp. 1087–1092, 1999.
[12] M. Inoue, K. Arai, T. Fujii, and M. Abe, "One-dimensional magnetophotonic crystals," *J. Appl. Phys.*, vol. 85, pp. 5768–5770, 1999.
[13] M. J. Steel, M. Levy, and R. M. Osgood, Jr., "High transmission enhanced Faraday rotation in one-dimensional photonic crystals with defects," *IEEE Photon. Technol. Lett.*, 1999, submitted for publication.
[14] D. Marcuse, *Theory of Dielectric Optical Waveguides*. Boston, MA: Academic, 1991.
[15] R. Wolfe, J. Hegarty, J. F. Dillon, Jr., L. C. Luther, G. K. Celler, and L. E. Trimble, "Magneto-optic waveguide isolators based on laser annealed (Bi, Ga) YIG films," *IEEE Trans. Magn.*, vol. MAG-21, pp. 1647–1650, 1985.
[16] R. Wolfe, R. A. Lieberman, V. J. Fratello, R. E. Scottie, and N. Kopylov, "Etch-tuned ridged waveguide magneto-optic isolator," *Appl. Phys. Lett.*, vol. 56, pp. 426–428, 1990.
[17] C. M. de Sterke, A. Arraf, L. Poladian, and T. G. Brown, "Effective-medium approach for counterpropagating waves in nonuniform Bragg gratings," *J. Opt. Soc. Amer. A*, vol. 14, pp. 1137–1143, 1997.
[18] M. Born and E. Wolf, *Principles of Optics*. Oxford, U.K.: Pergamon, 1989.
[19] M. Levy, R. Osgood, Jr., A. Kumar, and H. Bakhru, "Epitaxial liftoff of thin oxide layers: Yttrium iron garnets onto GaAs," *Appl. Phys. Lett.*, vol. 71, pp. 2617–2619, 1997.
[20] F. Rachford, M. Levy, R. Osgood, Jr., A. Kumar, and H. Bakhru, "Magnetization and FMR studies in implanted and crystal ion sliced Bi-YIG films," *J. Appl. Phys.*, vol. 85, p. 5217, 1999.
[21] H. Haus, *Waves and Fields in Optoelectronics*. Englewood Cliffs, NJ: Prentice-Hall, 1984.

M. J. Steel, photograph and biography not available at the time of publication.

M. Levy, photograph and biography not available at the time of publication.

R. M. Osgood, Jr. (SM'82–F'87), photograph and biography not available at the time of publication.